available at www.sciencedirect.com

ScienceDirect

journal homepage: www.elsevier.com/locate/jmbbm

Research paper

Computer simulation of elastic constants of hydroxyapatite and fluorapatite

E. Menéndez-Proupin[a], *S. Cervantes-Rodríguez*[b], *R. Osorio-Pulgar*[a], *M. Franco-Cisterna*[a], *H. Camacho-Montes*[c], *M.E. Fuentes*[b,*]

[a] *Departamento de Física, Facultad de Ciencias, Universidad de Chile, Las Palmeras 3425, 780-0024 Ñuñoa, Santiago, Chile*
[b] *Laboratorio de Química Computacional, Universidad Autónoma de Chihuahua, Campus Universitario II, 31125 Chihuahua, Mexico*
[c] *Basic Science Department, IIT, Universidad Autónoma de Ciudad Juarez, Av. Del Charro 460 norte Cd. Juarez, 32310 Chihuahua, Mexico*

ARTICLE INFO

Article history:
Received 15 November 2010
Received in revised form
24 February 2011
Accepted 1 March 2011
Published online 9 March 2011

Keywords:
Hydroxyapatite
Fluorapatite
Computer simulation
Stiffness constants

ABSTRACT

Hydroxyapatite (HAP) and fluorapatite (FAP) are essential components of dental enamel and bone. In this paper, we report a computational study of the elastic properties of HAP and FAP using ab initio and force field techniques. We have obtained the HAP and FAP elastic stiffness constants in hexagonal symmetry by fitting the Hooke law for both the energy–strain and stress–strain relations. Our ab initio HAP stiffness constants differ from the results of previous calculations, but follow similar trends. The HAP and FAP stiffness constants calculated with the ab initio method are very similar, although FAP is slightly stiffer than HAP in the hexagonal plane, and more compliant along the hexagonal axis. The pseudo-single-crystal HAP experimental stiffness constants in current use are critically reviewed. Combining the data from the ab initio simulations with the experimental FAP stiffness constants, several alternative sets of HAP stiffness constants are proposed. The mismatch in properties between HAP and FAP is evidently too small to assume it to be directly responsible for dental enamel mechanical degradation with fluorosis disease.

1. Introduction

Dental enamel is made up of apatitic mineralites (95–96 wt%), organic matter (1 wt%) and water (3 wt%) (Cuy et al., 2002). The majority of mineralized weaves needs multiscale modeling. Detailed composition and accurate structure–property relationships of apatitic mineralites are critically important for evaluating the mechanical properties of dental enamel. According to Baldazarri et al. (2008), small differences in material composition can lead to significant changes in mechanical properties. Among the most important crystals that comprise dental enamel are hydroxyapatite (HAP) and fluorapatite (FAP), with two formula units of $Ca_5(PO_4)_3(OH, F)$ per crystal cell. Modeling the mechanical properties of these compounds using electronic structure methods entails a description on the atomic scale of some characteristics of healthy and fluorotic teeth.

This study is motivated by a question about the influence of the composition of dental enamel on its mechanical properties. Topical fluoridation promotes ionic interchange in the external surface of HAP (non-prismatic enamel) that naturally exists on top of the enamel, converting it into a

* *Corresponding author.* Tel.: +52 614 1788201.
E-mail address: mfuentes@uach.mx (M.E. Fuentes).

1751-6161/$ - see front matter © 2011 Elsevier Ltd. All rights reserved.
doi:10.1016/j.jmbbm.2011.03.001

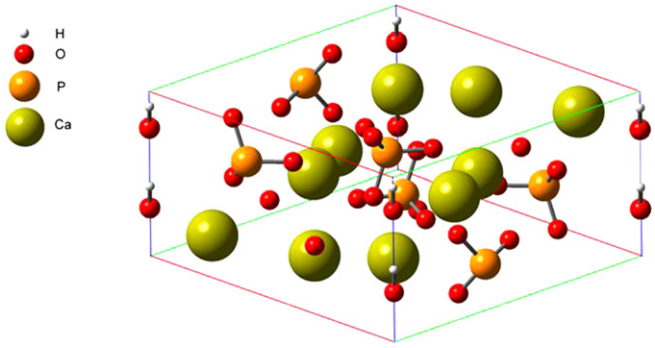

Fig. 1 – Schematic representation of an HAP unit cell.

hypermineralized surface of FAP (De Leeuw, 2002; Ten Cate, 1999). The demineralization–remineralization process that is enhanced through this mechanism is a worldwide exploited anti-caries technique.

This must not be confused with dental fluorosis, a disease mostly related to ingestion of water with excess fluoride. Although the existence of FAP crystals in the enamel internal tissue is not discarded in this cases, systemic fluoride mostly affects the dental amelogenesis process and does not provide real anti-caries protection (Aoba and Fejerskov, 2002). As a consequence, there are morphology, texture, and mineral/organic matrix proportion changes that could be related to the mechanical breakdown of fluorotic teeth, but they are not directly related to the atomic composition of the crystals.

The HAP crystal is mostly reported as a complex structure with 44 atoms in the hexagonal primitive cell (Chakraborty et al., 2006; Renaudin et al., 2008; Sänger and Kuhs, 1992), space group $P6_3/m$ and a 50% partial occupancy of the OH sites. It is schematically represented in Fig. 1. It is also found in the monoclinic space group $P2_1/b$, depending on the stoichiometry, temperature, and synthesis pressure (Snyders et al., 2007; Suetsugu et al., 2001; Suetsugu and Tanaka, 2002). Other subgroups of $P6_3/m$, i.e., $P2_1$ and $P6_3$, have been proposed, based on computational simulations (Haverty et al., 2005; Tofail et al., 2005). The differences between the different models are related to the local ordering of the OH^- groups and small distortion of the phosphate tetrahedra. A triclinic structure is also reported, being a small distortion from the $P6_3/m$ structure (Alberius-Henning et al., 2001).

FAP has a very similar structure, with 42 atoms in the unit cell, the same space group, and no partial occupancy (F^- anions instead of OH^- anions). The calcium ions in the apatite structure are in two different locations, Ca (1) and Ca (2). The Ca (1) ions, four per unit cell, are located far from the hexagonal axis that contains the F^- or OH^- anions and are surrounded by 6 oxygen atoms. The Ca (2) ions, six per unit cell, surround the channels of fluoride and hydroxyl ions in groups of three at different heights (Hughes et al., 1989).

Yoon and Newnham (1969) and Sha et al. (1994) measured the elastic stiffness constants of single-crystal FAP by means of ultrasonic techniques. Teraoka et al. (1998) measured the bending strength and Young's modulus of HAP single crystals. To our knowledge, there are no direct experimental reports of all the components of the stiffness tensor in HAP monocrystals that form dental enamel. Katz and Ukraincik (1971) performed an extended experimental analysis of FAP single crystals to derive a set of pseudo-single-crystal stiffness constants for HAP. Remarkably, the values determined in Katz and Ukraincik (1971) constitute the only approximation to "experimental" stiffness constants available today for HAP. Recently, Tofail et al. (2009) measured the elastic constants of a textured polycrystalline sample of HAP that has transverse isotropy. As a transversely isotropic medium has the same number of independent elastic constants as an hexagonal crystal, the monocrystal elastic constants can be derived from the polycrystal constants, although some assumptions are needed about how the monocrystal constants are averaged over the polycrystal (see Section 4 and the Appendix below).

There have been recent computational efforts devoted to the mechanical properties of this material (Ching et al., 2009; De Leeuw et al., 2007; Mostafa and Brown, 2007; Snyders et al., 2007). In De Leeuw et al. (2007) and Mostafa and Brown (2007), different force fields for the modeling of HAP and FAP were established based upon transferable potentials. The potentials were also used to calculate the compressibility data of HAP and FAP. Parameter-free ab initio calculations have been reported for HAP (Ching et al., 2009; Snyders et al., 2007), using density functional theory (DFT). However, the ab initio stiffness constants obtained in these calculations are significantly different.

In this article, we calculate the stiffness constants of HAP and FAP using DFT, and analyze the results in comparison with other DFT and force field calculations. In Section 2, we describe the structural models and the computational details. In Section 3, we present our results. In Section 4, we analyze the assumptions of Katz and Ukraincik (1971) and present new possible sets of stiffness constants for HAP. We also compare the properties of FAP and HAP. Section 5 is devoted to our conclusions.

2. Computational methods

2.1. *Structural models*

We studied the crystallographic structure of HAP refined by Hughes et al. (1989), as modified by Mostafa and Brown

(2007). The structure of Hughes et al. belongs to the $P6_3/m$ space group, with fractional occupation 0.5 for the OH groups. Mostafa and Brown expressed it in the P1 group and removed half of the OH groups. In fact, this structure has $P6_3$ symmetry.

The structure of FAP was taken from the experimental data in Hughes et al. (1989), already used as the starting structure in other computational studies (Mostafa and Brown, 2007; Tamm and Peld, 2006). It belongs to the $P6_3/m$ space group, with 42 atoms per unit cell. HAP also can be constructed similarly to FAP, substituting F atoms by the OH group.

Calderin et al. (2003) reported an electronic structure calculation of HAP. They obtained that the most stable HAP structure has the OH groups oriented in the same direction. They also simulated double unit cells with the hexagonal b cell doubled along the b direction, and found that the OH^- groups in neighboring cells can be parallel (hexagonal crystal) or antiparallel (monoclinic crystal), indistinguishable in terms of the total energy.

2.2. Elastic properties

The elastic stiffness constants are defined as

$$C_{ij} \equiv c_{\alpha\beta\gamma\delta} = \frac{1}{\Omega}\frac{\partial^2 E_{\text{total}}}{\partial\varepsilon_{\alpha\beta}\partial\varepsilon_{\gamma\delta}}, \tag{1}$$

where $U = E_{\text{total}}/\Omega$ is the total energy per unit volume, while $\sigma_{\alpha\beta}$ and $\varepsilon_{\alpha\beta}$ ($\alpha, \beta = x, y, z$) are the components of the stress and strain tensors, respectively. In the context of ab initio calculations, Ω is the unit cell volume, and E_{total} is the unit cell energy. The matrix of stiffness constants $C_{ij} = c_{\alpha\beta\gamma\delta}$ is defined by means of the Voigt compound indices $i = \alpha\beta, j = \gamma\delta$, following the rule $1 = xx, 2 = yy, 3 = zz, 4 = yz, 5 = zx, 6 = xy$. Due to the symmetry of hexagonal crystals, the matrix of stiffness constants of HAP and FAP can be expressed in terms of five independent constants: (Dieulesaint and Royer, 1980)

$$C = \begin{pmatrix} C_{11} & C_{12} & C_{13} & 0 & 0 & 0 \\ C_{12} & C_{11} & C_{13} & 0 & 0 & 0 \\ C_{13} & C_{13} & C_{33} & 0 & 0 & 0 \\ 0 & 0 & 0 & C_{44} & 0 & 0 \\ 0 & 0 & 0 & 0 & C_{44} & 0 \\ 0 & 0 & 0 & 0 & 0 & \dfrac{(C_{11}-C_{12})}{2} \end{pmatrix}. \tag{2}$$

The elastic properties can be characterized equivalently by the matrix of compliance constants S_{ij}, which is the inverse of the C matrix. The stress and strain tensors are symmetric, having only six independent components. This allows the Voigt notation, in which the stress and the strain are expressed as 6×1 matrices or their transposes:

$$\begin{aligned} S^T &= \begin{pmatrix} \sigma_{xx} & \sigma_{yy} & \sigma_{zz} & \sigma_{yz} & \sigma_{zx} & \sigma_{xy} \end{pmatrix}, \\ E^T &= \begin{pmatrix} \varepsilon_{xx} & \varepsilon_{yy} & \varepsilon_{zz} & 2\varepsilon_{yz} & 2\varepsilon_{zx} & 2\varepsilon_{xy} \end{pmatrix}. \end{aligned} \tag{3}$$

In the limit of infinitesimal deformation, the relationship between strain, stress, and energy can be expressed in matrix notation as

$$S = CE, \qquad U = \frac{E_{\text{total}}}{\Omega} = \frac{1}{2}E^T C E. \tag{4}$$

We used the periodic DFT method to calculate the energies and stress tensors of the HAP and FAP crystals subjected to strain. We applied five independent strains and fitted the stiffness constants to the energy–strain relations, as detailed in Table 1. For each type of strain, we calculated the total energy (E_{total}) for the values $\varepsilon_{\alpha\beta} = 0, \pm 0.0025, \pm 0.005, \pm 0.075, \pm 0.010$, and ± 0.015. The dependences $E_{\text{total}}(\varepsilon_{\alpha\beta})$ were fitted to polynomials of type

$$E_{\text{total}}(\varepsilon) = \Omega U(\varepsilon) = A_0 + A_1\varepsilon + A_2\varepsilon^2 + A_3\varepsilon^3. \tag{5}$$

The linear and cubic terms were necessary only in a few cases. A_1 corrects inaccuracies in the variable cell optimization, and A_3 corrects for anharmonic terms. The term A_2 was nonsensitive to the values of A_1, but the quality of the fit was improved. A_2/Ω is equal to $C_{11}/2$ for strain I, $C_{11} + C_{12}$ for strain II, etc., as in Table 1.

2.3. Ab initio total energy calculations

The total energy of the unit cell was calculated using the code QUANTUM ESPRESSO (Giannozzi et al., 2009), a plane wave and pseudopotential implementation of DFT (Kohanoff, 2006). In this framework, the total energy is the sum of the internuclear Coulomb repulsion and the electronic ground state energy in the field of the nuclei. The pseudopotential framework allows one to calculate only the states of the valence electrons, avoiding the explicit calculation of core states. In general, pseudopotential methods provide numerical results of the same quality as all-electron calculations. The electronic energy is obtained by solving the Kohn–Sham equations (Kohanoff, 2006). For the exchange and correlation interaction, we used the well-known PBE functional (Perdew et al., 1996). For the electron–core interaction, we used ultrasoft pseudopotentials (Vanderbilt, 1990).[1] We used a cutoff of 60 Ry for the plane wave expansion of the wavefunctions and 360 Ry for the charge density. We note that 60 Ry is an extremely high cutoff when ultrasoft pseudopotentials are used, but it was needed to obtain soft energy–strain curves. The first Brillouin zone was sampled with a $3\times3\times4$ k-point mesh centered at the Γ point and shifted half a step in the z-direction. With this setup, the energy, force, and pressure converged within 2 meV/atom, 3 meV/Å, and 0.4 kbar, respectively. The stress tensor in QUANTUM ESPRESSO is calculated based on the expressions derived by Nielsen and Martin (1983). This capability makes it possible to obtain the stiffness constants from the stress–strain relation (see Table 1). The elastic constants obtained from the stress–strain and energy–strain relations generally differ a little due to numerical issues, but these differences can be controlled by the convergence parameters mentioned above. Hence, comparing the values obtained by both methods allows us to assess the quality of the calculations.

Optimized (unstressed) structures were obtained using the variable-cell Parrinello–Rahman damped dynamics (Parrinello and Rahman, 1980), iterating until all the components

[1] We have used the pseudopotentials H.pbe-rrkjus.UPF, O.pbe-rrkjus.UPF, Ca.pbe-nsp-van.UPF, and P.pbe-n-van.UPF, from the QUANTUM ESPRESSO web site http://www.quantum-espresso.org.

Table 1 – Strains, and energy–strain and stress–strain relationships used to determine the elastic constants.

Name	Non-zero strain	Energy density	Non-zero stress
I	ε_{xx}	$U = \frac{1}{2}C_{11}\varepsilon_{xx}^2$	$\sigma_{xx} = C_{11}\varepsilon_{xx},\ \sigma_{yy} = C_{12}\varepsilon_{xx},\ \sigma_{zz} = C_{13}\varepsilon_{xx}$
II	$\varepsilon_{xx} = \varepsilon_{yy}$	$U = (C_{11} + C_{12})\varepsilon_{xx}^2$	$\sigma_{xx} = \sigma_{yy} = (C_{11} + C_{12})\varepsilon_{xx},\ \sigma_{zz} = 2C_{13}\varepsilon_{xx}$
III	ε_{zz}	$U = \frac{1}{2}C_{33}\varepsilon_{zz}^2$	$\sigma_{xx} = \sigma_{yy} = C_{13}\varepsilon_{zz},\ \sigma_{zz} = C_{33}\varepsilon_{zz}$
IV	$\varepsilon_{xx} = \varepsilon_{zz}$	$U = \frac{1}{2}(C_{11} + 2C_{13} + C_{33})\varepsilon_{xx}^2$	$\sigma_{xx} = (C_{11}+C_{13})\varepsilon_{xx},\ \sigma_{yy} = (C_{12}+C_{13})\varepsilon_{xx},\ \sigma_{zz} = (C_{13}+C_{33})\varepsilon_{xx}$
V	ε_{yz}	$U = 2C_{44}\varepsilon_{yz}^2$	$\sigma_{yz} = 2C_{44}\varepsilon_{yz}$

Table 2 – Crystallographic and theoretical lattice parameters of the structures of interest.

Material	a (Å)	b (Å)	c (Å)	c/a	α (°)	β (°)	γ (°)	Ω (Å^3)
			Theory					
HAP (this work)	9.582	9.580	6.879	0.72	90.00	90.00	120.00	546.85
HAP (this work) ($P = 29.18$ kbar)	9.435	9.435	6.850	0.73	90.00	90.00	120.00	528.01
FAP (this work)	9.509	9.509	6.898	0.73	90.00	90.00	119.99	540.18
FAP (this work) ($P = 22.76$ kbar)	9.406	9.406	6.866	0.73	90.00	90.00	120.00	526.05
HAP (Snyders et al., 2007)	9.635		6.595	0.68				530.20
HAP (Ching et al., 2009)	9.554		6.894	0.72				545.06
			Experiment					
HAP (Hughes et al., 1989)	9.418	9.416	6.875	0.73	90.01	89.99	119.94	527.99
FAP (Hughes et al., 1989)	9.398	9.397	6.878	0.73	89.99	90.02	120.06	526.04

of the stress tensor were smaller than 0.1 kbar, the total energy difference with the previous iteration was smaller than 1.4×10^{-5} eV (10^{-6} Ry), and the forces were smaller than 0.026 eV/Å (10^{-3} Ry/bohr). In the calculations to obtain the energy of the strained crystals, the atom positions were relaxed, using the same force and energy criteria as in the variable cell relaxations, and the BFGS algorithm implemented in QUANTUM ESPRESSO.

3. Results

3.1. *Relaxed structures*

Table 2 shows the crystallographic and theoretical lattice parameters. The HAP theoretical unit cell volume is 3.6% larger than the experimental reference volume, in agreement with the known trend of GGA predicting larger volumes than the experimental values. The theoretical volume of the FAP unit cell is 2.7% larger than that of the crystallographic FAP structure in Hughes et al. (1989).

3.2. *Elastic constants*

Fig. 2 shows the ab initio energy–strain data and the fitted curves for HAP. It can be observed that there is a well-defined relaxed structure energy minimum. Similar results are obtained for FAP. The stiffness constants obtained from the fits are listed in Tables 3 and 4. The fit is qualitatively very good, and this quality is reflected in the low estimated errors of the fitted constants, reported in brackets in Tables 3 and 4. Note that we dealt with energy differences as small as 1 meV. Although the absolute total energy has not converged, the energy differences are sufficiently converged to produce soft curves. Our initial calculations with a 35 Ry cutoff, typical for ultrasoft pseudopotentials, produced reasonable, but noisy curves. In some cases the strained cells had lower energy than the relaxed unit cell. Moreover, the 60 Ry cutoff allows a substantially better agreement between the stiffness constants fitted from the energy–strain and stress–strain data.

Only a few differences deserve to be mentioned between HAP and FAP. The FAP structure is more energy sensitive to elongational strain (ε_{11} and ε_{33}) and in-plane shear strain (ε_{12}) than both HAP structures, resulting in higher C_{11}, C_{33}, and C_{12} values for FAP. The situation for the out-of-plane shear strain (ε_{13} and ε_{44}) dependence for energy is observed to be the other way around, with lower C_{13} and C_{44} values for FAP.

It is well known that in GGA calculations the lattice parameters are overestimated with respect to room-temperature measurements. For HAP and FAP, the difference between the experiment values (Hughes et al., 1989) and our calculation values is 3.6% and 2.7%, respectively. The difference in unit cell volume is basically due to the a and b lattice parameters; the c parameter is almost equal in experiment and theory. To evaluate the effect of the lattice vector overestimation on the elastic constants, we have also calculated them imposing an external pressure that allows to reproduce the experimental unit cell volume.

Using classical force fields and the General Utility Lattice Package (GULP) (Gale and Rohl, 2003), it is also possible to obtain the elastic constants by using analytical derivatives of the energy against the strain tensor. We have explored this kind of model using the force fields of Mostafa and Brown (2007). The elastic constants can also be obtained by fitting the energy–strain curves. We used both types of calculation to check the reliability of our fitting procedure. The stiffness

Table 3 – HAP stiffness constants (in GPa). For each material, the constants in the first row have been fitted to the energy–strain relations. In the second row they have been fitted to the stress–strain relations. The fitting statistical error of the last digit is enclosed in brackets (two standard deviations).

	C_{11}	C_{12}	C_{13}	C_{33}	C_{44}	B[a]	G[a]
E versus strain	117.71(7)	31.1(1)	66.42(7)	165.0(1)	38.5(1)	77(4)	39.3(5)
Stress–strain	117.9(2)	30.55(7)	66.4(2)	165.0(2)	38.5(3)	77(4)	39.4(6)
Stress–strain ($P = 29.18$ kbar)	145.2(3)	47.8(1)	73.6(2)	191.4(2)	37.6(8)	95(2)	43.4(5)
Force fields (Mostafa and Brown, 2007)	158	57.5	59.8	147	43.9	90.77(3)	46.6(1)
Others: theory							
(Ching et al., 2009)	140.0	42.4	58.3	174.8	47.5	84.6(1.1)	47.6(1)
	134.8		60.1		47.6		
(Snyders et al., 2007)	117.1	26.2	55.6	231.8	56.4	76(6)	52(1)
(De Leeuw et al., 2007)	134.4	48.9	68.5	184.7	51.4	90(2)	46.6(4)
Experiments							
(Katz and Ukraincik, 1971)	137	42.5	54.9	172	39.6	82.6(8)	44.6(3)
Isotropic ceramic (Gilmore and Katz, 1982)						89[b]	44.5[b]
Textured ceramics[c] (Tofail et al., 2009)	137.2	53	55.1	123.2	42.2		
Monocrystal, from Voigt average[d]	123.2	51	59.2	138.8	48.3		
Monocrystal, from Reuss average[d]	123.6	51.6	59.5	139.6	50.9		

[a]Voigt–Reuss–Hill (VRH) averages of bulk (B) and shear (G) moduli calculated with the stiffness constants. Shown in parentheses is the difference between the VRH average and the Voigt and Reuss values, which are theoretical upper and lower limits, respectively.
[b]Experimental values.
[c]Experimental value for a textured transversely isotropic textured polycrystal sample.
[d]Derived from the experimental values on the textured isotropic polycrystal sample. See the Appendix for details.

Table 4 – FAP stiffness constants (in GPa). For each material, the constants in the first row have been fitted to the energy–strain relations. In the second row they have been fitted to the stress–strain relations. The fitting statistical error of the last digit is enclosed in brackets (two standard deviations).

	C_{11}	C_{12}	C_{13}	C_{33}	C_{44}	B[a]	G[a]
E versus strain	126.35(9)	36.2(2)	63.4(3)	167.6(2)	34(1)	81(2)	39.2(5)
Stress–strain	126.4(8)	35.8(3)	63.0(4)	167.7(5)	35(1)	81(2)	39.8(5)
Stress–strain ($P = 22.76$ kbar)	146.9(2)	48.4(1)	69.4(2)	188.2(2)	32(1)	94(2)	41(1)
Force fields (Mostafa and Brown, 2007)	165	55	60	145	40.2	91.6(1)	46.6(5)
Others: theory							
Force fields (De Leeuw et al., 2007)	150.6	62.8	73.6	176.6	53.2	99.2(6)	47.7(2)
Experiments							
(Yoon and Newnham, 1969)	143.4	44.5	57.5	180.5	41.5	86.5(9)	46.7(3)
(Gilmore and Katz, 1982)						94[b]	46.4[b]
(Sha et al., 1994)	152.0	49.7	63.1	185.8	42.8	92.8(8)	47.9(3)

[a]Voigt–Reuss–Hill (VRH) averages of bulk (B) and shear (G) moduli calculated with the stiffness constants. Shown in parentheses is the difference between the VRH average and the Voigt and Reuss values, which are theoretical upper and lower limits, respectively.
[b]Experimental values.

constants obtained by using analytical derivatives and by using our fitting procedure agree within 1%.

4. Discussion

Snyders et al. (2007) calculated the C_{ij} by the method of Fast et al. (1995), which is essentially our energy versus strain method. For comparison, the numerical parameters used in Snyders et al. (2007) were 495 eV cutoff, 0.01 meV SCF convergence in total energy, $7 \times 7 \times 7$ k-points, VASP code. Ching et al. (2009) used the stress–strain relations to calculate the C_{ij} by using finite differences. The stresses were obtained with VASP. However, they used stricter convergence criteria (notably a 600 eV cutoff). They obtained nine stiffness constants in total, which can be put in correspondence with the hexagonal symmetry constants using $(C_{11}+C_{22})/2 \to C_{11}$, $(C_{12}+C_{23})/2 \to C_{12}$, and $(C_{44}+C_{55})/2 \to C_{44}$.

The C_{ij} in Ching et al. (2009) are greater than ours, except C_{13}, and show better agreement with the values of Katz and Ukraincik (1971). However, as will be discussed below, this coincidence may be fortuitous. Snyders et al. (2007) obtained smaller C_{12} and C_{13} values than ours, but greater C_{33} and C_{44} values, averaging a similar bulk modulus and larger shear modulus compared to our calculation. Their results for C_{33} and C_{44} are more than 40% larger than our results, and

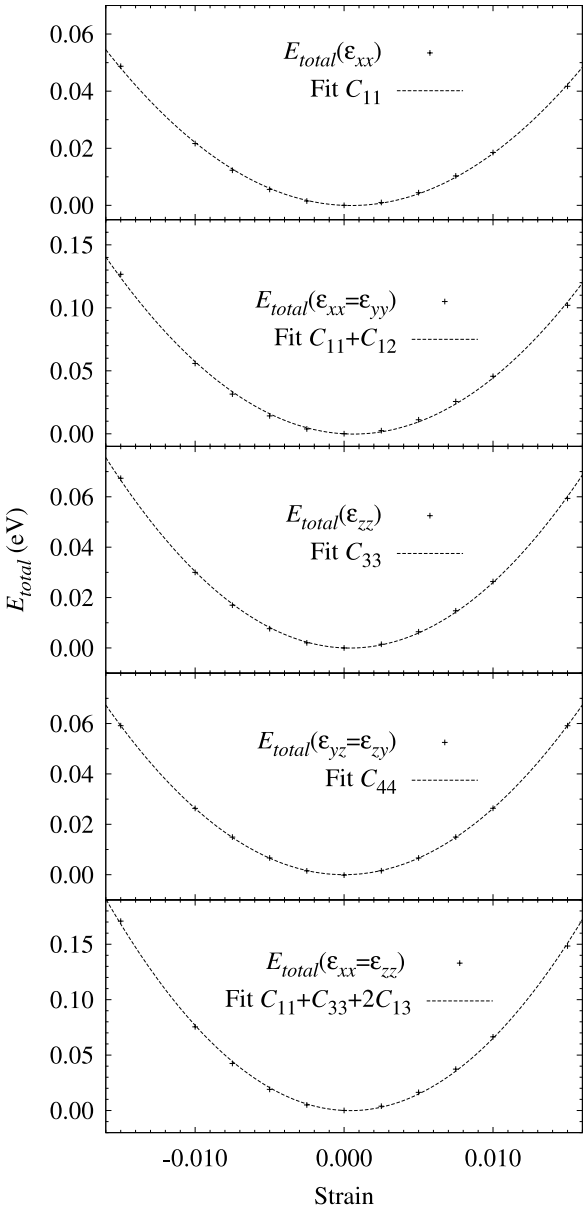

Fig. 2 – Ab initio energy versus strain data of HAP.

are also higher than those of all other calculations. They also obtained an anomalously low c/a ratio. It is difficult to assess the cause of the dispersion of the ab initio C_{ij} values, given that the three calculations share common methods. The three calculations used the periodic DFT approach, with plane wave basis sets and the GGA. Snyders et al. (2007) and Ching et al. (2009) used the same code, VASP; Snyders et al. used ultrasoft pseudopotentials, like us, while Ching et al. used the projector augmented wave potential. Ching et al. used the same functional as us, PBE, while Snyders et al. used a non-specified GGA functional, probably PW91 or PBE. These methodological differences generally produce marginal differences and do not explain the variability of the results. To discard the errors induced by different pseudopotentials and other implementation details, we have made test calculations of the C_{ij} constants using the VASP code. For the VASP calculations, we have used the set of parameters specified by Ching et al. (2009), and we have obtained the values C_{11} = 123 GPa, C_{12} = 34 GPa, C_{13} = 66 GPa, and C_{33} = 168 GPa, which are close to the values obtained with QUANTUM ESPRESSO. We have explored variations of the fitting procedure, the k-point grid, and 44-atom and 88-atom unit cells, and we have been unable to reproduce the results of Ching et al. (2009). Professor Ching has kindly supplied his refined structure with an orthorhombic unit cell, and we have obtained the same values for the elastic constants.

We have also tested a structural model with $P2_1/b$ symmetry derived from the crystallographic structure of Sänger and Kuhs (1992). This model has the same backbone with $P6_3/m$ symmetry, but the OH groups along the same line (c-axis) have opposite orientations, with the hydrogens pointing toward each other. The relaxed structure has a slightly higher energy (6 meV/atom) than the model described above. The elastic constants computed with both structures have no significant differences (less than 2.5 GPa).

Mostafa and Brown (2007) fitted empirical force fields to the structure and physical data of FAP, and used them to calculate the stiffness constants of HAP and FAP. Noting some errata in Mostafa and Brown (2007), we have recalculated the stiffness constants and have presented them in Tables 3 and 4. De Leeuw et al. (2007) have also fitted force fields to simulate a number of properties of apatites, including the elastic properties. For the sake of completeness, we include their results in Tables 3–5.

Comparing the ab initio stiffness constants of HAP and FAP with the experimental values, we observe that the C_{11}, C_{12}, and C_{33} values are significantly smaller than the experimental values, while C_{13} and C_{44} have larger or similar ab initio values.

The calculation with the external pressure produces higher stiffness constants except for C_{44}, which describes the response to shear stress. In the case of FAP, the pressure makes the values of C_{11}, C_{12}, and C_{33} fall within the values of the two reported experiments. In the case of HAP under pressure, all the stiffness constants except C_{44} are higher than the experimental values.

Van der Waals interaction, not reproduced by standard DFT (French et al., 2010), provides an additional attractive potential that contributes to reducing the unit cell volume and increasing the stiffness constants. In apatites, the dominant interactions are ionic and covalent, which are several orders of magnitude stronger than van der Waals interactions. An estimation of the van der Waals effect upon the elastic properties can be obtained from force field calculations (Mkhonto and de Leeuw, 2002), where dispersion terms of the form C/r^6 are fitted for the O–O, O–F and F–F pair potentials. When the FAP elastic constants are recalculated without the dispersion potentials, the elastic constants decrease by 2.2 GPa for C_{11} and C_{12} and less for the other constants. This is consistent with the known trend of van der Waals solids to have Young's moduli in the range 1–4 GPa (Ashby et al., 2007, p. 67). Hence, one can expect that a van der Waals corrected calculation may increase the stiffness constants by about 2 GPa.

The elastic constants obtained are typical of ionic solids (see, e.g., Catti et al., 1991). As shown by analysis of Mulliken

Table 5 – Ratio of the combinations of the stiffness constants assumed in Katz and Ukraincik (1971) to obtain the HAP pseudo-single-crystal stiffness constants, compared with the values obtained from simulations. Also are given the HAP stiffness constants (in GPa) as predicted with the method of Katz and Ukraincik (1971) using all the above ratios and the FAP experimental values of Yoon and Newnham (1969).

	Katz and Ukraincik (1971)	DFT	Force fields Mostafa and Brown (2007)	Force fields De Leeuw et al. (2007)
$\frac{(2C_{11}+C_{33})_{HAP}}{(2C_{11}+C_{33})_{FAP}}$	0.955	0.95	0.98	0.949
$\frac{(C_{12}+2C_{13})_{HAP}}{(C_{12}+2C_{13})_{FAP}}$	0.955	1.006	1.01	0.885
$\frac{((C_{11}-C_{12})/2+2C_{44})_{HAP}}{((C_{11}-C_{12})/2+2C_{44})_{FAP}}$	0.955	1.06	1.02	0.968
$\frac{(C_{11}+C_{12}-2C_{13})/(C_{33}-C_{13})_{HAP}}{(C_{11}+C_{12}-2C_{13})/(C_{33}-C_{13})_{FAP}}$	1.000	0.47	0.94	0.62
$\frac{2C_{44}/(C_{11}-C_{12})_{HAP}}{2C_{44}/(C_{11}-C_{12})_{FAP}}$	1.001	1.18	1.2	0.992
C_{11}	137	128[a]	137	128
C_{12}	42.5	33.6[a]	46.9	31.3
C_{13}	54.9	63.4[a]	57.2	54.9
C_{33}	172	189[a]	182	188
C_{44}	39.6	46.8[a]	45.1	40.1

[a] If the FAP stiffness constants determined by Sha et al. (1994) are used together with the DFT HAP/FAP ratios, then the predicted constants are as follows: $C_{11} = 136$ GPa, $C_{12} = 38.4$ GPa, $C_{13} = 69.3$ GPa, $C_{33} = 194$ GPa, and $C_{44} = 48.3$ GPa.

charges and bond orders (Rulis et al., 2004), FAP and HAP have strong covalent bonding within the phosphate and hydroxyl groups and ionic bonding between Ca^{2+}, PO_4^{3-}, F^-, and OH^-. Hence, according to the mechanical behavior, they can be regarded as ionic solids with complex ions.

Let us comment on the experimental stiffness constants. Gilmore and Katz (1982) obtained values of the bulk and shear moduli of dense polycrystalline HAP and FAP, as well as enamel and dentin, by measurement of the ultrasonic velocities in compressed powders with different pressures, and extrapolation to zero pressure to filter out the effect of porosity. For HAP, they obtained the values $B = 89.0$ GPa, $G = 44.5$ GPa, and $E = 114$ GPa. For FAP, $B = 94.0$ GPa, $G = 46.4$ GPa, and $E = 120$ GPa. The Young's modulus is calculated as $E = 9BG/(3B + G)$. They also showed that for composites HAP–NaCl, the Reuss approximation performs better than the Voigt one.

The experimental data reported by Yoon and Newnham (1969) and by Sha et al. (1994) for FAP provide the only experimental values of the elastic constants of fluorapatite to date. Katz and Ukraincik (1971) assumed that the single-crystal stiffnesses coefficients could be calculated for HAP by scaling the HAP isotropic moduli against the corresponding FAP moduli. They assumed that the combinations $2C_{11} + C_{33}$, $C_{12} + 2C_{13}$, and $(C_{11} - C_{12})/2 + 2C_{44}$ have a constant ratio HAP/FAP $= 0.955$, which is the average ratio of the measured bulk and shear moduli. These combinations appear in the Voigt averages, considering the symmetry constraints for the hexagonal group. Katz and Ukraincik also assumed that $(C_{11} + C_{12} - 2C_{13})/(C_{33} - C_{13})$ and $2C_{44}/(C_{11} - C_{12})$ take the same values in both FAP and HAP crystals. Solving the equations, they determined the pseudo-single-crystal stiffness constants of HAP. However, the measured bulk modulus values for both FAP and HAP are inconsistent with the Voigt bulk moduli determined from the single-crystal stiffness constants. In fact, they are out of the range between the Reuss and Voigt values. Moreover, Table 5 shows the HAP/FAP ratios of the combinations of the stiffness constants used in Katz and Ukraincik (1971), and the values obtained from simulations with ab initio and force field models. It can be seen that some of the ratios deviate considerably from the values assumed in Katz and Ukraincik (1971). Finally, using the ratios given by the simulations, we have recalculated the HAP stiffness constants with the method of Katz and Ukraincik (1971), and we have presented them in Table 5.

Recently, Tofail et al. (2009) have measured the elastic constants of a textured sample of HAP, such that the hexagonal axes of the grains are aligned in the XY-plane of the sample, and arbitrarily oriented within this plane. This sample had transverse isotropic symmetry. The elastic constants of the textured material can be estimated by averages of the stiffness tensor (Voigt averages) and by averages of the compliance tensor (Reuss averages), as discussed in the Appendix. As the transversely isotropic medium has the same number of independent elastic constants as the hexagonal crystal, the above equations can be easily solved to obtain the monocrystal stiffness constants from the polycrystal constants. Table 3 shows the monocrystal stiffness constants derived from the polycrystal constants assuming the Voigt and Reuss conditions. A comparison between the estimated monocrystal properties and Katz and Ukraincik data shows a somewhat unexpected disagreement, also showing the scattering of the experimental data in the literature due to difficulties in obtaining accurate measurements. The newly derived C_{11} value is smaller than the Katz and Ukraincik values and closer to the ab initio value. The C_{33} value is also smaller than the Katz and Ukraincik values, with the DFT values in between. The C_{12} and C_{44} values are higher than both other values. The C_{13} value is between the DFT and Katz and Ukraincik values.

In all the experimental and theoretical results, the differences between corresponding C_{ij} values and unit cell parameters of HAP and FAP are too small to entail any dramatical change in tooth mechanical properties. They do not seem to be directly responsible for mechanical breakdowns in enamel with fluorosis. In accordance with the results of Baldazarri et al. (2008), the existence of residual organic matrix in dental

enamel seems the most important factor because of the mechanical mismatch between ceramics and organic materials. Nevertheless, the question of the influence of the morphology and texture of polycrystalline structures remains open. As a tendency verified by all the cited methods, hyper-mineralized enamel surfaces containing large amounts of FAP could be more rigid than purely HAP compositions.

5. Conclusions

We have presented a first-principles calculation of the elastic stiffness constants of FAP and HAP. We have studied the effect of the alternative HAP structures on the stiffness constants. We have discussed the dispersion of the stiffness constants calculated by different authors using similar methods. The DFT stiffness constant values are, in general, significantly smaller than the experimental values, with the exception of C_{13}. Setting an empirical external pressure to reproduce the experimental unit cell density allows us to improve the elastic constants for FAP, giving values that fall between the two available experimental measurements. However, in the case of HAP, the external pressure does not improve the agreement with experimental values of the stiffness constants. Hence, purely ab initio methodology is currently unable to predict accurate values of the HAP elastic constants (or there is a very wide range for them). Nevertheless, the experimental values of HAP elastic constants are based on measurements in polycrystalline samples and differ by as much as 24%. However, DFT reproduces the experimental findings of Sha et al. (1994) and Yoon and Newnham (1969) about the anisotropy, i.e., C_{33}/C_{11}. Moreover, combining the data from our ab initio calculations with the experimental FAP data, we have recalculated the HAP pseudo-single-crystal stiffness constants, providing updated and reasonable values. In the new sets of HAP stiffness constants, the C_{13}, C_{33}, and C_{44} values are larger than the old values (Katz and Ukraincik, 1971), while and C_{11} and C_{12} are similar. We hope that our results stimulate efforts to measure the single-crystal elastic constants of HAP precisely. Regarding the problem of dental enamel, the mismatch in elastic properties between HAP and FAP seems to be too small to explain the degradation of mechanical properties with fluorosis disease. The influence of residual organic matrix, crystal morphology, and texture can be more reasonable causes for mechanical degradation, and this remains an open topic for investigation.

Acknowledgements

This work was supported by Programa Bicentenario de Ciencia y Tecnología (Chile) Grant No. ACT/ADI-24 and CONACYT (Mexico) Grant No. 25380 and Grant No. 100559. We also acknowledge N. Mostafa for help in reproducing calculations, and S. Baroni for useful comments. M.E.F. is grateful to Centro Nacional de Supercómputo, IPICYT, and D. Rios-Jara for invaluable computational support.

Appendix. Elastic constants of polycrystalline apatites

In isotropic, non-textured, polycrystalline materials, there are only two independent elastic constants, the bulk (B) and shear (G) moduli. Other constants like the Young's modulus, Poisson ratio, and Lamé coefficients are expressed in terms of B and G. Isotropic moduli are averages of the elastic constants of the monocrystals, but the also depend on the way that individual grains interact with each other.

Upper and lower bounds for the bulk and shear moduli can be easily calculated if it is assumed that either the strain or the stress is continuous across grain boundaries. Assuming continuous strain, one obtains the Voigt averages (Nye, 1957):

$$B_{\text{Voigt}} = \frac{1}{9}\left[C_{11} + C_{22} + C_{33} + 2\left(C_{12} + C_{13} + C_{23}\right)\right] \tag{6}$$

$$G_{\text{Voigt}} = \frac{1}{15}\left[C_{11} + C_{22} + C_{33} + 3\left(C_{44} + C_{55} + C_{66}\right) - C_{12} - C_{13} - C_{23}\right]. \tag{7}$$

If the stress is assumed to be continuous across the grain boundaries, the Reuss average values are

$$B_{\text{Reuss}} = \left[S_{11} + S_{22} + S_{33} + 2\left(S_{12} + S_{13} + S_{23}\right)\right]^{-1} \tag{8}$$

$$G_{\text{Reuss}} = 15\left[4\left(S_{11} + S_{22} + S_{33} - S_{12} - S_{13} - S_{23}\right) + 3\left(S_{44} + S_{55} + S_{66}\right)\right]^{-1}, \tag{9}$$

where C_{ij} and S_{ij} are the components of the stiffness matrix defined in Eq. (1) and its inverse (i.e., the compliance matrix). The Voigt–Reuss–Hill elastic moduli are the arithmetic averages of the Voigt and Reuss values, and are generally considered to be a better approximation to the experimental values.

In a textured polycrystal, the function $f(\phi, \theta, \psi)$ describes the probability of having grains with the principal crystal axes rotated with respect to reference axes, the rotation being described by Euler angles (ϕ, θ, ψ). The stiffness tensor of a rotated monocrystal expressed in reference axes is given as

$$c_{\alpha\beta\gamma\delta}(\phi, \theta, \psi) = \sum_{\alpha', \beta', \gamma', \delta' = 1}^{3} a_{\alpha\alpha'} a_{\beta\beta'} a_{\gamma\gamma'} a_{\delta\delta'} c_{\alpha'\beta'\gamma'\delta'},$$

where $c_{\alpha'\beta'\gamma'\delta'}$ is the tensor expressed in the principal axes of the crystal (Eq. (2)), and $a_{\mu\nu}$ is the Euler rotation matrix $a(\phi, \theta, \psi)$, given in Box I.

A Voigt average can be cast as

$$\left\langle c_{\alpha\beta\gamma\delta}\right\rangle_{\text{V}} = \int_0^{2\pi}\int_0^{\pi}\int_0^{2\pi} f(\phi, \theta, \psi)\, c_{\alpha\beta\gamma\delta}(\phi, \theta\psi) \times \sin\theta \mathrm{d}\phi \mathrm{d}\theta \mathrm{d}\psi.$$

A Reuss average results from application of the same transformations to the compliance tensor. The standard Voigt and Reuss averages for non-textured polycrystals are obtained when $f(\phi, \theta, \psi) = 1/8\pi^2$. With these transformations, the stiffness and compliance tensors become isotropic, and using the relations $B = (C_{11} + 2C_{12})/3 = 1/(3S_{11} + 6S_{12})$ and $G = C_{44} = 1/S_{44}$, with C_{ij} and S_{ij} being the averaged constants, Eqs. (6)–(9) are obtained.

For a textured sample of HAP, such that the hexagonal axes of the grains are aligned in the XY-plane of the sample, and arbitrarily oriented within this plane (Tofail et al., 2009),

$$a(\phi,\theta,\psi)=\begin{pmatrix}\cos\phi\cos\psi-\cos\theta\sin\phi\sin\psi & -\cos\psi\sin\phi-\cos\theta\cos\phi\sin\psi & \sin\theta\sin\psi\\ \cos\theta\cos\psi\sin\phi+\cos\phi\sin\psi & \cos\theta\cos\phi\cos\psi-\sin\phi\sin\psi & -\cos\psi\sin\theta\\ \sin\theta\sin\phi & \cos\phi\sin\theta & \cos\theta\end{pmatrix}.$$

Box I.

we can consider $f(\phi,\theta,\psi)=\delta(\theta-\pi/2)/4\pi^2$. This sample has transversely isotropic symmetry. The Voigt averages for this texture are

$$C_{11}^{\text{Voigt}}=\frac{1}{8}\left(3C_{11}+2C_{13}+3C_{33}+4C_{44}\right)$$
$$C_{12}^{\text{Voigt}}=\frac{1}{8}\left(C_{11}+6C_{13}+C_{33}-4C_{44}\right)$$
$$C_{13}^{\text{Voigt}}=\frac{1}{2}\left(C_{12}+C_{13}\right)$$
$$C_{33}^{\text{Voigt}}=C_{11}$$
$$C_{44}^{\text{Voigt}}=\frac{1}{4}\left(C_{11}-C_{12}+2C_{44}\right)$$

and the Reuss averages of the compliance constants are

$$S_{11}^{\text{Reuss}}=\frac{1}{8}\left(3S_{11}+2S_{13}+3S_{33}+S_{44}\right)$$
$$S_{12}^{\text{Reuss}}=\frac{1}{8}\left(S_{11}+6S_{13}+S_{33}-S_{44}\right)$$
$$S_{13}^{\text{Reuss}}=\frac{1}{2}\left(S_{12}+S_{13}\right)$$
$$S_{33}^{\text{Reuss}}=S_{11}$$
$$S_{44}^{\text{Reuss}}=S_{11}-S_{12}+\frac{S_{44}}{2}.$$

The asymmetry between the averages of C_{ij} and S_{ij} is easily understood, considering their relations with the corresponding tensors, $C_{44}=c_{2323}$ versus $S_{44}=4s_{2323}$, which in turn originate in the different way in which the strain and stress tensors enter in the Voigt notation, i.e., Eq. (3).

REFERENCES

Alberius-Henning, P., Adolfsson, E., Grins, J., Fitch, A., 2001. Triclinic oxy-hydroxyapatite. J. Mater. Sci. 36, 663–668.

Aoba, T., Fejerskov, O., 2002. Dental fluorosis: chemistry and biology. Crit. Rev. Oral. Biol. Med. 13, 155–170.

Ashby, M.F., Shercliff, H., Cebon, D., 2007. Materials: Engineering, Science, Processing and Design. Butterworth-Heinemann, Oxford.

Baldazarri, M., Margolis, H.C., Beniash, E., 2008. Compositional determinants of mechanical properties of enamel. J. Dent. Res. 87, 645–649.

Calderin, L., Stott, M.J., Rubio, A., 2003. Electronic and crystallographic structure of apatites. Phys. Rev. B 67, 134106-1-7.

Catti, M., Dovesi, R., Pavese, A., Saunders, V.R., 1991. Elastic constants and electronic structure of fluorite (CaF2): an ab initio Hartree–Fock study. J. Phys.: Condens. Matter 3, 4151–4164.

Chakraborty, S., Bag, S., Pal, S., Mukherjee, A.K., 2006. Structural and microstructural characterization of bioapatites and synthetic hydroxyapatite using X-ray powder diffraction and Fourier transform infrared techniques. J. Appl. Crystallogr. 39, 385–390.

Ching, W.Y., Rulis, P., Misra, A., 2009. Ab initio elastic properties and tensile strength of crystalline hydroxyapatite. Acta Biomater. 5, 3067–3075.

Cuy, J.L., Mann, A.B., Livi, K.J., Teaford, M.F., Weihs, T.P., 2002. Nanoindentation mapping of the mechanical properties of human molar tooth enamel. Arch. Oral Biol. 47, 281–291.

De Leeuw, N.H., 2002. Density functional theory calculations of local ordering of hydroxy groups and fluoride ions in hydroxyapatite. Phys. Chem. Chem. Phys. 4, 3865–3871.

De Leeuw, N.H., Bowe, J.R., Rabone, J., 2007. A computational investigation of stoichiometric and calcium-deficient oxy- and hydroxy-apatites. Faraday Discuss. 134, 195–214.

Dieulesaint, E., Royer, D., 1980. Elastic Waves in Solids. Wiley, Chichester.

Fast, L., Wills, J.M., Johansson, B., Eriksson, O., 1995. Elastic constants of hexagonal transition metals: theory. Phys. Rev. B 51, 17431–17438.

French, R.H., Parsegian, V.A., Podgornik, R., Rajter, R.F., Jagota, A., Luo, J., Asthagiri, D., Chaudhury, M.K., Granick, S., Kalinin, S., Kardar, M., Kjellander, R., Langreth, D.C., Lewis, J., Lustig, S., Wesolowski, D., Wettlaufer, J.S., Ching, W.-Y., Finnis, M., Houlihan, F., von Lilienfeld, O.A., van Oss, C.J., Zemb, T., 2010. Long range interactions in nanoscale science. Rev. Modern Phys. 82, 1887–1944.

Gale, J., Rohl, A., 2003. The general utility lattice program (GULP). Mol. Simul. 29, 291–341.

Giannozzi, P., Baroni, S., Bonini, N., Calandra, M., Car, R., Cavazzoni, C., Ceresoli, D., Chiarotti, G., Cococcioni, M., Dabo, I., Dal Corso, A., de Gironcoli, S., Fabris, S., Fratesi, G., Gebauer, R., Gerstmann, U., Gougoussis, C., Kokalj, A., Lazzeri, M., Martin-Samos, L., Marzari, N., Mauri, F., Mazzarello, R., Paolini, S., Pasquarello, A., Paulatto, L., Sbraccia, C., Scandolo, S., Sclauzero, G., Seitsonen, A., Smogunov, A., Umari, P., Wentzcovitch, R., 2009. QUANTUM ESPRESSO: a modular and open-source software project for quantum simulations of materials. J. Phys.: Condens. Matter. 21, 395502-1-19.

Gilmore, R.S., Katz, J.L., 1982. Elastic properties of apatites. J. Mater. Sci. 17, 1131–1141.

Haverty, D., Tofail, S.A.M., Stanton, K.T., McMonagle, J.B., 2005. Structure and stability of hydroxyapatite: density functional calculation and Rietveld analysis. Phys. Rev. B 71, 094103-1-9.

Hughes, C.M., Cameron, M., Crowley, K., 1989. Structural variations in natural F, OH, and Cl apatites. Am. Mineral. 74, 870–876.

Katz, J.L., Ukraincik, K., 1971. On the anisotropic elastic properties of hydroxyapatite. J. Biomech. 4, 221–227.

Kohanoff, J., 2006. Electronic Structure Calculations for Solids and Molecules: Theory and Computational Methods. Cambridge University Press, Cambridge.

Mkhonto, D., de Leeuw, N.H., 2002. A computer modelling study of the effect of water on the surface structure and morphology of fluorapatite: introducing a $Ca_{10}(PO_4)F_2$ potential model. J. Mater. Chem. 12, 2633–2642.

Mostafa, N.Y., Brown, P.W., 2007. Computer simulation of stoichiometric hydroxyapatite: structure and substitutions. J. Phys. Chem. Solids 68, 431–437.

Nielsen, O.H., Martin, R.M., 1983. First-principles calculation of stress. Phys. Rev. Lett. 50, 697–700.

Nye, J.F., 1957. Physical Properties of Crystals. Oxford University Press, New York.

Parrinello, M., Rahman, A., 1980. Crystal structure and pair potentials: a molecular-dynamics study. Phys. Rev. Lett. 45, 1196–1199.

Perdew, J.P., Burke, K., Ernzerhof, M., 1996. Generalized gradient approximation made simple. Phys. Rev. Lett. 77, 3865–3868.

Renaudin, G., Laquerriere, P., Filinchuk, Y., Jallot, E., Nedelec, J.M., 2008. Structural characterization of sol–gel derived Sr-substituted calcium phosphates with anti-osteoporotic and anti-inflammatory properties. J. Mater. Chem. 18, 3593–3600.

Rulis, P., Ouyang, L., Ching, W.Y., 2004. Electronic structure and bonding in calcium apatite crystals: hydroxyapatite, fluorapatite, chlorapatite, and bromapatite. Phys. Rev. B 70, 155104.

Sänger, A.T., Kuhs, W.F., 1992. Z. Kristallogr. 199, 123–148.

Sha, M., Li, Z., Bradt, R.C., 1994. Single-crystal elastic constants of fluorapatite, $Ca_5F(PO_4)_3$. J. Appl. Phys. 75, 7784–7787.

Snyders, R., Music, D., Sigumonrong, D., Schelnberger, B., Jensen, J., Schneider, J.M., 2007. Experimental and ab initio study of the mechanical properties of hydroxyapatite. Appl. Phys. Lett. 90, 193902-1-3.

Suetsugu, Y., Ikoma, T., Tanaka, J., 2001. Single crystal growth and structure analysis of monoclinic hydroxyapatite. Key Eng. Mater. 192, 287–290.

Suetsugu, Y., Tanaka, J., 2002. Crystal growth and structure analysis of twin-free monoclinic hydroxyapatite. J. Mater. Sci., Mater. Med. 13, 767–772.

Tamm, T., Peld, M., 2006. Computational study of cation substitutions in apatites. J. Solid State Chem. 179, 1581–1587.

Ten Cate, J.M., 1999. Current concepts on the theories of the mechanism of action of fluoride. Acta Odontol. Scand. 57, 325–329.

Teraoka, K., Ito, A., Maekawal, K., Onuma, K., Tateishi, T., Tsutsumi, S., 1998. Mechanical properties of hydroxyapatite and OH-carbonated hydroxyapatite single crystals. J. Dent. Res. 77, 1560–1568.

Tofail, S.A.M., Haverty, D., Cox, F., Erhart, J., Hána, P., Ryzhenko, V., 2009. Direct and ultrasonic measurements of macroscopic piezoelectricity in sintered hydroxyapatite. J. Appl. Phys. 105, 064103-1-5.

Tofail, S.A.M., Haverty, D., Stanton, K.T., McMonagle, J.B., 2005. Structural order and dielectric behaviour of hydroxyapatite. Ferroelectrics 319, 117–123.

Vanderbilt, D., 1990. Soft self-consistent pseudopotentials in a generalized eigenvalue formalism. Phys. Rev. B 41, 7892–7895.

Yoon, H.S., Newnham, R.E., 1969. Elastic properties of fluorapatite. Am. Mineral. 54, 1193–1197.